Global Change Biology

Global Change Biology (2017) **23**, 2482–2498, doi: 10.1111/gcb.13542

Predicting vegetation type through physiological and environmental interactions with leaf traits: evergreen and deciduous forests in an earth system modeling framework

ENSHENG WENG[1], CAROLINE E. FARRIOR[2], RAY DYBZINSKI[3] and STEPHEN W. PACALA[1]

[1]*Department of Ecology & Evolutionary Biology, Princeton University, Princeton, NJ 08544, USA,* [2]*Department of Integrative Biology, University of Texas at Austin, Austin, TX 78712, USA,* [3]*Institute of Environmental Sustainability, Loyola University Chicago, Chicago, IL 60660, USA*

Abstract

Earth system models are incorporating plant trait diversity into their land components to better predict vegetation dynamics in a changing climate. However, extant plant trait distributions will not allow extrapolations to novel community assemblages in future climates, which will require a mechanistic understanding of the trade-offs that determine trait diversity. In this study, we show how physiological trade-offs involving leaf mass per unit area (LMA), leaf lifespan, leaf nitrogen, and leaf respiration may explain the distribution patterns of evergreen and deciduous trees in the temperate and boreal zones based on (1) an evolutionary analysis of a simple mathematical model and (2) simulation experiments of an individual-based dynamic vegetation model (i.e., LM3-PPA). The evolutionary analysis shows that these leaf traits set up a trade-off between carbon- and nitrogen-use efficiency at the scale of individual trees and therefore determine competitively dominant leaf strategies. As soil nitrogen availability increases, the dominant leaf strategy switches from one that is high in nitrogen-use efficiency to one that is high in carbon-use efficiency or, equivalently, from high-LMA/long-lived leaves (i.e., evergreen) to low-LMA/short-lived leaves (i.e., deciduous). In a region of intermediate soil nitrogen availability, the dominant leaf strategy may be either deciduous or evergreen depending on the initial conditions of plant trait abundance (i.e., founder controlled) due to feedbacks of leaf traits on soil nitrogen mineralization through litter quality. Simulated successional patterns by LM3-PPA from the leaf physiological trade-offs are consistent with observed successional dynamics of evergreen and deciduous forests at three sites spanning the temperate to boreal zones.

Keywords: dynamic global vegetation model, evolutionarily stable strategy, forest succession, game theory, leaf traits, LM3-PPA, nitrogen cycle

Received 3 April 2016; revised version received 17 October 2016 and accepted 18 October 2016

Introduction

Dynamic global vegetation models (DGVMs) are widely used in Earth system models as the land components for simulating interactions between climate and vegetation. The biodiversity of global vegetation is represented by a set of plant functional types (PFTs) in DGVMs: usually a small collection of trees, shrubs, and grasses based on the canonical biomes of the world (Prentice *et al.*, 1992). The parameters of each PFT are assigned according to the biome-wide averages of plant traits and the *extant* temperature and precipitation relationships (e.g., LPJ, Sitch *et al.*, 2003). This approach made it possible to predict global vegetation dynamically and to simulate the interactions between climate and vegetation when data and computational power were limited (Foley *et al.*, 1998, 2000). However, the use of PFTs underrepresents the variation in plant traits and artificially constrains vegetation processes, which may increase the uncertainty of model predictions (Scheiter *et al.*, 2013; Wullschleger *et al.*, 2014).

Significant advances have been made recently in uncovering the most ubiquitous between-species correlations among traits and between traits and environmental conditions (Wright *et al.*, 2004, 2005; Osnas *et al.*, 2013; Reich *et al.*, 2014) and in documenting how trait distributions change during community assembly (Shipley *et al.*, 2006; Weiher *et al.*, 2011; Laughlin & Laughlin, 2013). These studies make it possible to improve plant functional diversity in DGVMs for realistically simulating vegetation dynamics. A straightforward approach is to directly add the empirical relationships between climate and plant traits into the models. Simulation results have shown that this approach improves model realism and predictions (e.g., Wang *et al.*, 2012; Verheijen *et al.*, 2013, 2015; Reich *et al.*, 2014). Moreover, plant traits, together with

Correspondence: Ensheng Weng, tel. +1 609 258 6886, fax 609 258 6818, e-mail: wengensheng@gmail.com

theories of community assembly, can be used to predict vegetation dynamics and distribution based on environmental constraints (Kleidon & Mooney, 2000) and plant competition (van Bodegom *et al*., 2014; Violle *et al*., 2014).

Individual and trait-based DGVMs that link plant traits and individual physiological and demographic processes together to predict vegetation dynamics have been developed, for example, aDGVM2 (Scheiter *et al*., 2013), JeDi-DGVM (Kleidon & Mooney, 2000; Reu *et al*., 2011; Pavlick *et al*., 2013), ED (Moorcroft *et al*., 2001; Medvigy *et al*., 2009), and LPJmL-FIT (Sakschewski *et al*., 2015). These models simulate competition for limited resources among individuals and can compete a large number of PFTs – now defined by combinations of plant traits – against one another to determine the most competitive trait mix. In doing so, they predict the correlations between plant traits and climate that emerge from numerical simulations (e.g., Pavlick *et al*., 2013; Scheiter *et al*., 2013; Sakschewski *et al*., 2015).

However, including extant relationships between climate and plant traits will not necessarily reduce model uncertainties (e.g., Pappas *et al*., 2016) because novel community assemblages may emerge in the future as they did with past climate change (Davis, 1986). By definition, novel community assemblages have no current observations from which to draw parameter values (Ackerly, 2003). In addition, numerical simulations of the individual- and trait-based models are unlikely by themselves to produce a mechanistic understanding of the way in which traits determine the outcome of competition for different resources, in part because of the limited number of strategies that can be competed against one another in practice and in part because of the complexity of the problem (Farrior *et al*., 2013b; Pappas *et al*., 2016).

The simulation results and behavior of individual-based models can be explained by game theoretic analyses (Maynard Smith, 1974). Game theoretic approaches have been employed to solve mathematically for the most competitive trait combination(s) in a continuous multivariate trait distribution, such as the competitively optimal biomass allocation among leaves, stems, and fine roots (Dybzinski *et al*., 2011, 2013, 2015; Farrior *et al*., 2013a,b), crown depth (Vermeulen, 2014), tree height (King, 1990; Falster & Westoby, 2003), leaf angles (Hikosaka & Hirose, 1997), and leaf area index (LAI; Anten, 2002). Although game theoretic mathematical analyses have been useful in explaining field observations and experimental results (e.g., Dybzinski *et al*., 2013; Farrior *et al*., 2013b) and improving our understanding of simulation results from complex models (e.g., Weng *et al*., 2015), their obvious disadvantage is the model simplicity they require.

In this study, we base our model on observed trade-offs among leaf traits and use both approaches – game theoretic analysis of a simplified mathematical model and simulation experiments using the land component of an earth system model (LM3-PPA, Weng *et al*., 2015) – to investigate how leaf traits affect the outcome of competition among evergreen and deciduous vegetation types in mesic environments across the temperate and boreal zones. Throughout, we use the terms 'mathematical model' and 'simulation experiments' to differentiate these approaches (even though the simulations require mathematics as well).

Briefly, we formulate a 'universe of possible plant types' based on the trade-offs between leaf mass per unit area (LMA) and other leaf traits (including leaf lifespan, leaf nitrogen, leaf respiration, and litter decomposition rate) and compete combinations against one another under conditions of limiting nitrogen and light. Using the mathematical model, we predict both the conceptually useful 'optimal' LMA that maximizes carbon (C) gain given an *extrinsic* nitrogen (N) mineralization rate as well as the more ecologically relevant 'competitively dominant' (evolutionarily stable strategy, ESS) LMA that cannot be invaded by any other strategy when explicitly including feedbacks of leaf traits on N mineralization. We show that the results qualitatively explain the mix of evergreen and deciduous forest types observed across the varying N availability in soils in temperate and boreal regions. Finally, we use the corresponding version of LM3-PPA to predict forest structure and dynamics at three sites in the temperate and boreal regions.

Materials and methods

Physiological trade-offs in leaf traits

Studies of interspecific variation in leaf traits show the critical role played by LMA (Wright *et al*., 2004; Lloyd *et al*., 2013; Osnas *et al*., 2013). LMA is positively correlated with leaf lifespan, area-based leaf N content, and leaf respiration rate (Osnas *et al*., 2013) and negatively correlated with mass-based leaf N content (Wright *et al*., 2004). We hypothesize that these correlations are trade-offs created by physical constraints and evolution. An increase in the potential lifespan of a leaf likely requires additional functional and structural tissues and thus increases LMA. The additional tissues in high-LMA leaves then must contain some N and respire because more mesophyll cells are in high-LMA leaves (Evans & Poorter, 2001; Osnas *et al*., 2013; Villar *et al*., 2013). However, the N content of the added structural material is low, meaning the ratio of C : N increases with LMA (Wright *et al*., 2004; Osnas *et al*., 2013), which decreases the rate of biomass decomposition (Mcclaugherty *et al*., 1985; Garnier *et al*., 2004; Cornwell *et al*., 2008). These hypotheses form the basis of the model:

1. Leaf lifespan (λ, year) is proportional to LMA (σ, kgC m^{-2}) (Wright *et al*., 2004; Osnas *et al*., 2013):

$$\lambda = c\sigma, \tag{1}$$

where c is a constant (yr kgC^{-1} m^2).

2. Leaf N content per unit leaf area (n, gN m^{-2}) is a linear function of LMA (Osnas *et al*., 2013):

$$n = A + B\sigma, \tag{2}$$

where A (gN m^{-2}) and B (gN kgC^{-1}) are constants. Osnas *et al*. (2013) showed that for most species A is larger than $B\sigma$, likely because most leaf N is distributed proportional to area due to its role in photosynthesis.

3. Leaf respiration rate (R, kgC m^{-2} yr^{-1}) is proportional to leaf nitrogen (Reich *et al*., 1998b).

$$R = nr = (A + B\sigma)r, \tag{3}$$

where r is a constant (kgC gN^{-1} yr^{-1}).

4. The residence time of soil organic matter (SOM) (τ_s, year) is linearly related to the LMA of a forest stand's leaf litter (Cornwell *et al*., 2008; Zhang *et al*., 2008):

$$\tau_s = \xi(T, M)s^*\sigma, \tag{4}$$

where $\xi(T, M)$ (unitless) is a function of soil temperature (T) and moisture (M) that modifies the decomposition rate of SOM. The parameter, s^*, is a constant (yr kgC^{-1} m^2). Note that we assume a zero intercept in this relationship (Eqn 4) in the mathematical model, but qualitatively similar results are obtained with a nonzero intercept.

These four equations assume linear relationships among the leaf traits and SOM decomposition and set up the trade-offs for cost-benefit and competitive analysis. To explore the sensitivity of our model to these trade-offs, we analyzed the effects of alternative nonlinear monotonic functional forms of the two major trade-offs, leaf lifespan vs. LMA and respiration vs. leaf nitrogen, on model predictions.

Mathematical model of canopy net carbon gain

In addition to the aforementioned trade-offs among leaf traits, we incorporate a series of other assumptions in the mathematical model to represent the processes of photosynthesis, respiration, and decomposition. For convenience, the mathematical model assumes that ecosystems are N-limited. That is, annual leaf production is limited by annual N mineralization rate. Because trees use roughly half of their yearly N uptake to construct new leaves and retranslocate roughly half of leaf N before leaves drop (Dybzinski *et al*., 2011, 2015), leaf N per unit ground area will equilibrate approximately at the product of soil N mineralization rate and leaf lifespan in an N-limited monotypic forest with a closed canopy. So the N-limited LAI is:

$$L = \frac{N_m\lambda}{n} = \frac{N_m c\sigma}{A + B\sigma}, \tag{5}$$

where L is N-limited LAI and N_m is annual N mineralization rate (gN m^{-2} yr^{-1}). According to this equation, the N-limited LAI increases monotonically with LMA (Fig. 1a, parameters in Table 1).

We assume that annual C fixation (photosynthesis) is an exponentially saturating function of LAI, a well-established approach used in light-use efficiency models (Monteith, 1977; Landsberg & Waring, 1997; Duursma & Makela, 2007):

$$C_{gain} = \frac{V}{k}(1 - e^{-kL}), \tag{6}$$

where C_{gain} is annual C fixation (kgC m^{-2} yr^{-1}), V is the per unit leaf area productivity of a leaf in full sun (kgC m^{-2} yr^{-1}), and the constant k captures the effect of self-shading of leaves within a plant's crown on C_{gain}. Because we are testing the effects of variation in LMA on leaf dominant strategy, we set a constant photosynthetic capacity for all the leaves (constant parameter V), regardless of their LMA. This assumption is consistent with the observation that the maximum rate of photosynthesis per unit leaf area and LMA are independent (Osnas *et al*., 2013). Note C_{gain} does depend indirectly on LMA here, however, as LAI is a function of LMA (Eqn 5).

Annual C cost per unit crown area of a tree's canopy (C_{cost}, kgC m^{-2} yr^{-1}) is the sum of maintenance and building costs of the leaves:

$$C_{cost} = \left(R + G\frac{\sigma}{\lambda}\right)L = N_m rc\sigma + G\frac{\sigma N_m}{A + B\sigma}, \tag{7}$$

where G is building cost per unit leaf mass (kgC kgC^{-1}), including both the carbon used for constructing the leaves and the respiration of growth itself. Taken together, the net C gain of a canopy (C_{net}, kgC m^{-2} yr^{-1}) is the difference between the canopy C fixation (i.e., C_{gain}) and the C cost of leaves:

$$C_{net} = \frac{V}{k}\left(1 - e^{-k\frac{N_m c\sigma}{A+B\sigma}}\right) - N_m rc\sigma - \frac{G\sigma N_m}{A + B\sigma}. \tag{8}$$

To illustrate the plant-level trade-offs of the model's leaf-level physiology, we plot the dependence of LAI, C_{gain}, C_{cost}, and C_{net} on LMA in Fig. 1 using parameters in Table 1.

For simplicity of the N cycle in the mathematical model, we assume that all plant N uptake is used in leaves (instead of half), and eliminate N retranslocation before leaf drop (instead of the half in retranslocation). Conveniently, these effects cancel and all equations derived above remain unchanged with this simplification. At equilibrium, the N mineralization rate (N_m, gN m^{-2} yr^{-1}) can then be expressed as a function of total ecosystem N (N_{total}, gN m^{-2}) and the residence times of N in the leaves (λ) and soil (τ_s):

$$N_m = \frac{N_{total}}{\lambda + \tau_s} = \frac{N_{total}}{[c + \xi(T, M)s^*]\sigma_R} = \frac{N_{total}}{(c + s)\sigma_R}, \tag{9}$$

where $s = \xi(T, M)s^*$, and σ_R is the average leaf LMA of the stand's leaf litter or the LMA of the monodominant 'resident' trees. (See Eqs. S31–S33 in Appendix S2 for the mathematical derivation.)

We analyze this framework mathematically to predict dominant leaf traits of plants across soil nitrogen gradients due to both total ecosystem N and climate. First, we find the optimal strategy as a function of an *extrinsic* environmental N mineralization rate. Second, we find the

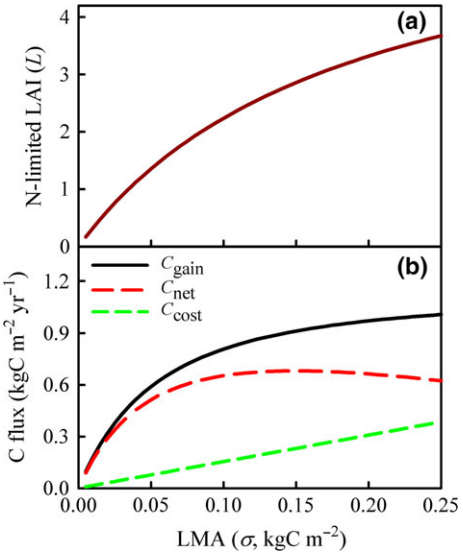

Fig. 1 Fundamental assumptions and predictions of the mathematical model. (a) N-limited leaf area index (L) as a function of LMA (Eqn 5). (b) The dependence of canopy-level carbon (C) gain (C_{gain}), C cost (C_{cost}), and net canopy C gain (C_{net}) on LMA following Eqns (6–8). Although C_{gain} saturates with LMA, C_{cost} increases almost linearly, resulting in C_{net} maximization at an intermediate value of LMA (optimal LMA).

competitively dominant or ESS given feedbacks between dominant species LMA and the N_m, which includes the feedback between leaf nitrogen and the litter decomposition rate. For both of these analyses, and like many previous studies (Field, 1983; Pearcy *et al.*, 1987; Goetz & Prince, 1999), we assume that net C gain (Eqn 8) is proportional to fitness. Note, to compute the ESS LMA (σ_{ESS}), we assume that successive invasions are sufficiently far apart enough in time for the N mineralization rate to equilibrate to the resident strategy with LMA σ_R (Eqn 9).

We assume potential invaders are rare (i.e., they have a negligible effect on N_m). Thus, the net C gain of an invader with LMA, σ_I, is as follows:

$$C_{net}(\sigma_I|\sigma_R) = \frac{V}{k}\left(1 - e^{-k\cdot(N_m(\sigma_R)c\sigma_I)/(A+B\sigma_I)}\right) - N_m(\sigma_R)rc\sigma_I - \frac{G\sigma_I N_m(\sigma_R)}{A+B\sigma_I}, \quad (10)$$

where $N_m(\sigma_R)$ is the annual N mineralization rate determined by the resident. To find the σ_{ESS}, we differentiate the right-hand side of Eqn (10) with respect to σ_I, replace both σ_I and σ_R in the resulting expression by σ_{ESS}, and solve for σ_{ESS}.

The solution here is not sufficient to prove that σ_{ESS} is a true ESS because the solution could be the least competitive strategy (a minimum) or invadable by strategies not nearby in strategy space (i.e., not a *global* maximum) (Geritz *et al.*, 1998). So, in addition to the analytical calculations of σ_{ESS}, we also explore the invasion problem numerically to validate the analytical solutions. We evaluate C_{net} ($\sigma_I|\sigma_R$) and C_{net} ($\sigma_R|\sigma_R$) for all possible combinations of 1000 values of σ_I and σ_R ranging from 0.00005 to 0.5 at intervals of 0.00005, to determine which invaders successfully invade each resident LMA (invasion succeeds if C_{net} ($\sigma_I|\sigma_R$) > C_{net} ($\sigma_R|\sigma_R$)) (Fig. S1). The resulting pairwise invasion plot can be interpreted to determine whether σ_{ESS} is a global, convergence-stable maximum. Parameter values for these calculations are in Table 1. The leaf parameters in this table are adapted from the data of leaf traits studies (e.g., Reich *et al.*, 1998a, 1999; Wright *et al.*, 2004). Other parameters, such as photosynthetic capacity and soil C residence time, are based on relevant studies in North American temperate forests (e.g., Curtis *et al.*, 2002; Lichter *et al.*, 2008). These parameters are for numerically illustrating the quantitative patterns of the model and thus can be varied within reasonable ranges without changing the results.

In one of the cases considered below, any resident LMA below a critical value can always be invaded by a smaller LMA (Fig. S1d). This is unrealistic at the limit of low LMA, where clearly zero LMA is not a feasible plant strategy. This result comes from the simplified assumption that photosynthetic capacity V and functional N per unit area A (Eqn 2) are both constant. In the limit of low LMA, this may not be true because the low LMA may reduce the functional N and therefore reduce photosynthetic capacity. This necessitates the introduction of a boundary ESS. An ESS on a boundary constraint cannot be invaded by any trait value near to, but not on the boundary. Because any possible leaf must contain essential

Table 1 Parameter values used by the mathematical model to illustrate the quantitative patterns of N-limited leaf area index, canopy carbon gain, carbon cost, net carbon gain, optimal leaf mass per area (LMA), and competitively dominant LMA (i.e., evolutionarily stable strategy, ESS)

Parameter	Description	Value	Unit
c	Leaf lifespan parameter (Eqn 1)	28.57	yr kgC^{-1} m^2
A	Functional leaf N (Eqn 2)	1.5	gN m^{-2}
B	Structural leaf N (Eqn 2)	8	gN kgC^{-1}
r	Leaf respiration parameter (Eqn 3)	0.015	kgC gN^{-1} yr^{-1}
V	Photosynthesis parameter (Eqn 6)	1.2	kgC m^{-2} yr^{-1}
k	Saturate rate of GPP with LAI (Eqn 6)	0.5	–
G	Growth carbon cost (Eqn 7)	1.3333	kgC kgC^{-1}
s	Soil N residence time parameter (Eqn 9)	500	yr kgC m^{-2}
σ_{min}	Minimum leaf mass per unit area (Eqn 13)	0.02	kgC m^{-2}

structures such as an epidermis, palisade layer, and transport system, we introduce a minimum possible LMA, σ_{min}, to constrain the boundary ESS at a plausible value (0.02 kgC m^{-2}, Table 1). It is close to the lower limit of maple tree's LMA as shown in GLOPNET data (Wright *et al.*, 2004).

LM3-PPA and nitrogen cycle model

In order to study the potential for the leaf trait trade-offs (Eqns 1–3) to predict the emergent property of forest succession and distribution, we use the newly developed LM3-PPA (Weng *et al.*, 2015) for simulation experiments. LM3-PPA is based on an explicit scaling of individual plants to ecosystems. Its energy, CO_2, and water dynamics are fully coupled to an atmospheric model, but it can also be run offline with climate forcing data. LM3-PPA includes height-structured competition for light and root allocation-dependent competition for both water and nitrogen. The representation of individual trees allows LM3-PPA to predict forest structure and succession mechanistically.

We incorporate a simple N cycle model (Fig. 2) into LM3-PPA to simulate ecosystem N dynamics based on those developed by Gerber *et al.* (2010) and Manzoni *et al.* (2010). In LM3-PPA, an individual tree has six C pools: leaves, fine roots, sapwood, heartwood, fecundity (seeds), and nonstructural carbohydrates (NSC). We add an N pool corresponding to each of these (Fig. 2). The N absorbed by roots enters the nonstructural N (NSN) pool first and then is allocated to the remaining plant pools during plant growth. The details and parameters can be found in Appendix S1 and Table S1.

In LM3-PPA, there is a target LAI that helps plants to manage NSC allocation (Weng *et al.*, 2015). Given the possibilities of N-limitation and N-saturation in this study, we replaced the target LAI with the minimum of two targets: an N-limited target and a light-limited target. The N-limited target is calculated following the rationale of Eqn (5) by LMA, leaf lifespan, leaf N, and an annual N mineralization index (see Eqs. S4 and S5 in Appendix S1). It is updated once per modeled year. The light-limited target is the value that causes a tree's most shaded leaves to have lifetime gross primary production (GPP) approximately equal to the total lifetime construction and respiratory costs of a leaf and its supportive tissues (i.e., sapwood and roots). It is precomputed for canopy trees of each PFT. The light-limited target can only be reached when N is saturating. Flows from NSN to new tissues simply piggyback on the carbon allocation as described in Weng *et al.* (2015), but using the new target LAI formulation (details are in Appendix S1).

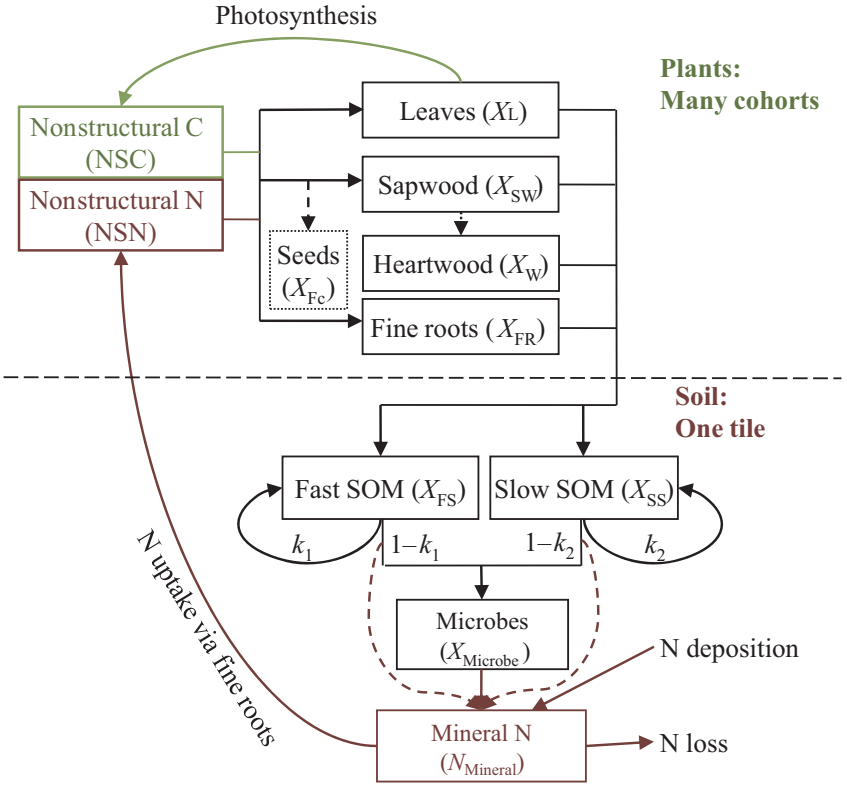

Fig. 2 Schematic diagram of the coupling of carbon and N cycles in LM3-PPA. The green, brown, and black lines are the flows of carbon, nitrogen, and coupled carbon and nitrogen, respectively. The green box is for carbon only. The brown boxes are N pools. The black boxes are for both carbon and nitrogen pools, where *X* can be C (carbon) and N (nitrogen). The C : N ratios of leaves, fine roots, and microbes are fixed. Only one tree's C and N pools are shown in this figure. The model can have multiple cohorts of trees, which share the same pool structure. The dashed line separates the plant and soil processes.

Because soil microbes may be limited by either C or N, soil N mineralization does not simply piggyback on the decomposition processes of SOM. The SOM decomposition model in Weng *et al.* (2015) is replaced with one that includes interacting N and C dynamics belowground (see detail in Appendix S1). It is coupled to the soil physics and hydrology models to allow it to capture the dependence of decomposition on soil temperature and moisture and the leaching losses of mineralized N dependent on runoff.

Simulated experiments with LM3-PPA

In simulation experiments, we defined two PFTs using the leaf trait relationships (Eqns 1–3). We used red maple (*Acer rubrum* L.) as the source for parameter values unrelated to LMA and its effects because red maple was used for test runs in LM3-PPA (Weng *et al.*, 2015). One PFT had LMA = 0.035 kgC m^{-2}, giving it a leaf lifespan that qualifies as deciduous; the other had LMA = 0.175 kgC m^{-2}, giving it a leaf lifespan that qualifies 'evergreen' (quotation marks acknowledging the background red maple parameter values, Table 2). We set the parameters A, B, c, and r in Eqns (1–3) (Table 2) so that the leaves of the deciduous PFT had the same leaf lifespan, photosynthesis rate, and respiration rate as the red maple in Weng *et al.* (2015), where the parameters of red maple were adapted from the literature (e.g., Abrams, 1998; Nagel *et al.*, 2002) and tuned according to simulations.

These two PFTs differ from one another only in LMA, leaf lifespan (from Eqn 1), leaf N per unit area (from Eqn 2), and leaf respiration per unit area (from Eqn 3). We did not incorporate the differences in stems and roots between deciduous and evergreen trees because they did not change the trade-offs involving leaf traits. Our simulations were designed to isolate the community- and ecosystem-level consequences of trade-offs among leaf traits alone. The constancy in parameters unrelated to LMA allows us to focus the analysis of model results on LMA and its effects specifically.

The precomputed light-limited target LAIs were 3 and 4 for the 'evergreen' and deciduous PFTs, respectively. The deciduous is higher than the 'evergreen' because the respiration of low-LMA leaves is lower than that of high-LMA leaves. Because we use a constant parameter of respiration for all the leaves within a canopy, the respiration cost is overestimated for leaves in lower layers of a canopy, leading to an underestimation of light-limited LAI in this study. But this does not have a qualitative effect on the results. Light-limited target LAIs for all understory trees were set to 1.2.

Because the maximum rate of carboxylation (V_{max}) in the photosynthesis model of Weng *et al.* (2015) is thought to be proportional to photosynthetic N per unit leaf area (Medlyn *et al.*, 1999; Kattge *et al.*, 2009), we assume that it is proportional to the functional N concentration A of Eqn (2):

$$V_{max} = aA, \tag{11}$$

where a is a constant (μmolC s^{-1} gN^{-1}). Also, we replace the leaf maintenance respiration in Weng *et al.* (2015), which is proportional to V_{max}, with Eqn (3). Because parameter A does not change with LMA, V_{max} does not vary with LMA. This is consistent with the assumption of a constant V in the mathematical model. All parameter values not given in Weng *et al.* (2015) can be found in Table 2.

We conducted two classes of simulation experiments: one with three different levels of fixed total ecosystem N at one site and one with an open N cycle including atmospheric deposition and leaching at three sites (Table 3). Every simulation includes the two PFTs defined above. These simulation experiments were designed to show how leaf trait relationships (leaf lifespan vs. LMA, leaf N vs. LMA, and leaf respiration vs. leaf N) allow a complex DGVM to predict successional patterns in temperate and boreal zones.

The three closed N cycle simulation experiments used climate drivers for Harvard Forest (HFR) and had total N levels of 170, 310, and 710 gN m^{-2}, respectively, without N deposition and loss. The sites for the open N cycle simulation experiments covered different biomes in North America: deciduous forest at Oak Ridge (OKR) (Norby *et al.*, 2001), mixed confer–deciduous forest at Harvard Forest (HFR) (Savage & Davidson, 2001), and evergreen conifer forest at the Northern Old Boreal forest site in Manitoba, Canada (NOBS) (Bergeron *et al.*, 2007; Dunn *et al.*, 2007). The latitudes of these sites range from 35°N to 55°N and the yearly mean temperatures are 13.9 °C, 8.5 °C, and −3.2 °C, respectively (Table 3). We used the Sheffield climate data set (Sheffield *et al.*, 2006) from the grid cells covering the three sites

Table 2 Parameter values used by the LM3-PPA model to simulate competition between deciduous and evergreen trees and forest succession

Parameters	Description	Value	Unit
σ_D	Deciduous LMA	0.035	kgC m^{-2}
σ_E	Evergreen LMA	0.175	kgC m^{-2}
A	Functional N	1.5	gN m^{-2}
B	Structural N	8	gN kgC^{-1}
c	Leaf lifespan parameter	28.57	yr kgC^{-1} m^2
a	Photosynthesis parameter (Eqn 11)	3.125×10^{-4}	μmolC s^{-1} gN^{-1}
r_0	Respiration parameter	3.5×10^{-7}	kgC gN^{-1} s^{-1}
N_{input}	Annual N input	0.8	gN m^{-2} yr^{-1}
$L_{light,D}$	Light-limited LAI of deciduous trees	4.0	m^2 m^{-2}
$L_{light,E}$	Light-limited LAI of evergreen trees	3.0	m^2 m^{-2}

to drive the LM3-PPA model. In the open N cycle runs, the atmospheric deposition rate was set as 0.8 gN m^{-2} yr^{-1}, added to the mineral N pool in daily increments. Initial conditions for all runs are in Tables S2 and S3.

Results

'Optimal' and evolutionarily stable strategy LMA in the mathematical model

In the mathematical model, the net C gain is a decreasing function of LMA because respiration per unit leaf area increases with LMA (Eqn 3), whereas photosynthesis per unit area is independent of LMA. Also, the annualized carbon construction cost of a unit of leaf area is also independent of LMA ((LMA/Leaf life span) = $1/c$, Eqn 1). Putting these together, the net C return per unit C invested in leaves increases as LMA decreases. In contrast, a unit of low-LMA leaf area requires more N to produce than a unit of high-LMA leaf area, because the annualized N cost of a unit of leaf area is as follows: (Leaf N/Leaf life span) = $(A/c\sigma)$ $+(B/c)$ (see Eqns 1 and 2). Thus, low-LMA plants should be best in N-rich environments, where the N does not significantly constrain LAI (Eqn 5) because low-LMA leaves have the highest C return per unit C invested. High-LMA plants should be best in N-poor environments, where their significantly higher LAI overwhelms their disadvantage in carbon return per unit carbon invested in each leaf layer.

The optimal LMA, σ^*, which assumes a fixed extrinsic N mineralization rate (i.e., no feedback between LMA and mineralization rates), is found by setting the derivative of Eqn (8) with respect to σ equal to zero. The resulting expression contains an implicit solution for σ^*:

$$N_m = \frac{A + B\sigma^*}{kc\sigma^*} \ln\left[\frac{V}{(A + B\sigma^*)^2 r/A + G/c}\right]. \quad (12)$$

This equation is not analytically solvable for σ^* as a function of N_m, but it is straightforward to prove that $dN_m/d\sigma^* < 0$. That is, optimal LMA (σ^*) decreases as the N mineralization rate increases, thus favoring deciduous species in N-rich soils (Fig. 3a).

The most competitive LMA (σ_{ESS}), which allows for feedbacks between LMA and N mineralization rates, is found by substituting the right-hand side of Eqn (9) into the left-hand side of Eqn (12) and setting the resident LMA equal to the optimal LMA ($\sigma_R = \sigma^*$) according to the definition of ESS. The resulting expression contains an implicit solution for σ_{ESS} as a function of N_{total} (see Eq. S35 in Appendix S2). Because the required N_{total} for a σ_{ESS} varies with environmental factors (e.g., temperature and soil moisture), we define a 'reference' N mineralization rate (N_m^{ref}) where the resident LMA is normalized to σ_{min} (0.02 kgC m^{-2}) and the total N meets the N requirement of a σ_{ESS} at given temperature and soil moisture:

$$N_m^{ref} = \frac{N_{total}}{(c+s)\cdot\sigma_{min}} = \frac{(A + B\sigma_{ESS})}{kc\,\sigma_{min}} \ln\left(\frac{V}{(A + B\sigma_{ESS})^2 r/A + G/c}\right). \quad (13)$$

Thus, N_m^{ref} has two meanings: As an index of N requirement of a σ_{ESS}, it is solely determined by leaf traits and independent of environmental factors (i.e., temperature and soil moisture), and as an index of N availability that determines σ_{ESS}, it integrates the influences of environmental factors on N availability. Like Eqn (12), this equation cannot be solved analytically for the ESS LMA on the right-hand side, but unlike

Table 3 Locations, vegetation types, major tree species, and climatic conditions of the three forest sites for simulation experiments of LM3-PPA (Data are from the AmeriFlux website http://ameriflux.ornl.gov/.)

	Oak Ridge/Walker Branch (OKR)	Harvard Forest (HFR)	Northern Old Black Spruce site (NOBS)
Location	Tennessee, USA	Massachusetts, USA	Manitoba, Canada
Coordinates (Lat., Long.)	35.96°, −84.29°	42.54°, −72.18°	55.88°, −98.48°
Vegetation type	Deciduous broadleaf forest	Deciduous broadleaf/mixed forest	Evergreen needleleaf forest
Major species	Oaks (*Quercus alba*, *Quercus prinus*), hickory (*Carya ovata*), red maple (*Acer rubrum*), *tulip poplar* (*Liriodendron tulipifera*), and loblolly pine (*Pinus taeda*)	Red oak (*Quercus rubra*), red maple (*Acer rubrum*), black birch (*Betula lenta*), white pine (*Pinus strobes*), hemlock (*Tsuga canadensis*)	Black spruce (*Picea mariana*)
Annual precipitation (mm)	1371	1050	517
Yearly mean temperature (°C)	13.9	8.5	−3.2

Eqn (12), the right-hand side of Eqn (13) is a nonmonotonic function of LMA (Fig. 3).

Numerical solutions for ESS LMA (σ_{ESS}) given by Eqn (13) using the parameters in Table 1 reveal that solutions fall into three cases (Fig. 3b), delimited by N_m^{ref}:

Case 1, 'Evergreen'. If N_m^{ref} is less than a threshold value N_1, then there is a single convergence-stable ESS with relatively large LMA and leaf lifespan. This threshold value is as follows:

$$N_1 = \frac{(A + B\sigma_{min})}{kc\,\sigma_{min}} \ln\left(\frac{V}{(A + B\sigma_{min})^2 r/A + G/c}\right). \quad (14)$$

Invasion tests confirm that this ESS is both global and convergence stable (see Fig. S1 for invasion tests). Theoretically, the maximum value of σ_{ESS} given by the intercept of the vertical axis in Fig. 3b is as follows:

$$\sigma_{ESS,max} = \left(\sqrt{\frac{V - G/c}{rA}} - 1\right) A/B. \quad (15)$$

Case 2, 'Bistable'. If N_m^{ref} is greater than N_1 and less than a value N_2 in Fig. 3b, then there are two stable ESSs, one at a relatively large value and one at the lower boundary value σ_{min} (Fig. 3b). These two ESSs are separated by an uninvadable but convergence-*unstable* point, and so indicate founder control. If the LMA of the initial resident type is below this convergence-unstable point, then a series of successful invasions by ever smaller LMAs leads to the boundary ESS, σ_{min}, with its minimum leaf lifespan, highly decomposable litter, and a high N mineralization rate. In contrast, if the initial LMA is above this convergence-unstable point, then a series of invasions leads to the upper ESS, with relatively long-leaf lifespan, recalcitrant leaf litter, and a low N mineralization rate.

The upper threshold N_2 can be approximated by the following equation (see Appendix S2 for mathematical derivation):

$$N_2 \approx \frac{A}{ekc\,\sigma_{min}} \sqrt{\frac{V}{rA}} \ln\left(\frac{V}{V/e^2 + G/c}\right). \quad (16)$$

Case 3, 'Deciduous'. If N_m^{ref} is greater than N_2, then there is a single ESS at the minimum value σ_{min} (the brown line in Fig. 3b).

The above three cases qualitatively predict the distributions of deciduous and evergreen trees in mesic temperate and boreal regions. Because N_m^{ref} increases with both N_{total} and temperature (s in the denominator decreases as temperature increases, Eqn 13), competitively dominant LMA (i.e., σ_{ESS}) depends on both environmental factors and total N (Fig. S2). Trees with short-leaf lifespans (low LMA) are predicted to be the endpoint of succession in warm regions, unless soil N is low, whereas species with long-lived leaves (high LMA) dominate in cold regions unless soil N is particularly high. The prediction of both evergreen and deciduous forests under intermediate conditions is caused by founder control, driven by the litter feedback of LMA on N mineralization through changing litter quality. The high C : N of leaf litter, associated with high LMA, leads to low N mineralization (Eqn 4), which reinforces the competitive advantage of long-leaf lifespan, high-LMA leaves in N-poor habitats (Eqn 13). Similarly, low leaf C : N leads to high N mineralization, reinforcing the competitive advantage of short-leaf lifespan/low-LMA leaves in N-rich habitats (the high net C return per unit C invested in leaves).

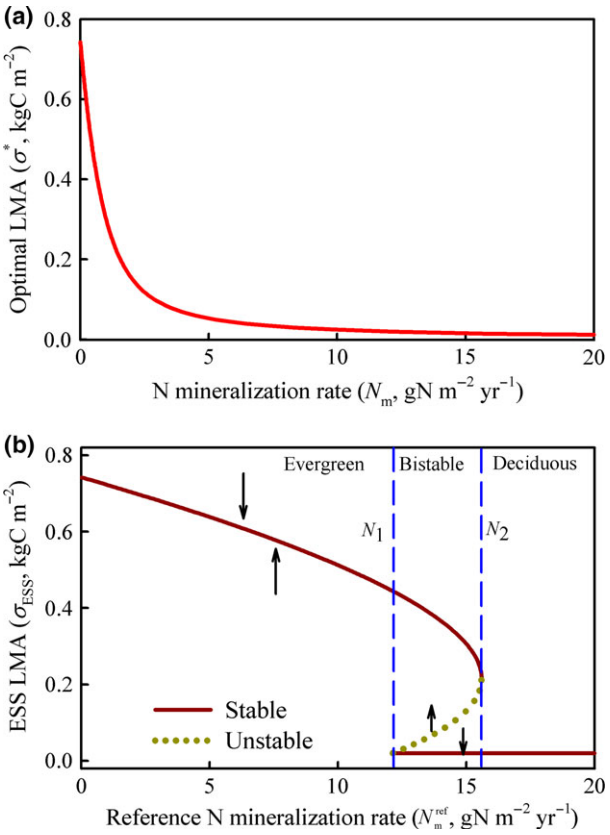

Fig. 3 Optimal LMA (a) and the evolutionarily stable strategy (ESS) of LMA (b). (a) The dependence of 'optimal' LMA on N mineralization rate, assuming no feedback between LMA and the nitrogen mineralization rate (N_m, Eqn 12). (b) The dependence of ESS LMA (σ_{ESS}) on N availability is captured by reference N mineralization rate (N_m^{ref}, Eqn 13). Reference N mineralization rate integrates the total ecosystem N (N_{total}) and the effects of temperature and moisture at LMA equal to σ_{min} (0.02 kgC m^{-2}). Brown indicates convergence-stable local ESSs. Green shows the unstable equilibrium and N_1 and N_2 mark two critical thresholds of N_m^{ref} that mark change in predicted dominant forest types (Eqns 14 and 16).

Sensitivity of ESS LMA to alternative leaf trait trade-offs

We have assumed a linear relationship between LMA and leaf lifespan (Eqn 1). Although this relationship is strong in empirical data, there is also considerable residual variation (Wright *et al.*, 2005). We analyze the impact of this uncertainty on the predicted ESS by assuming a power law for the LMA–leaf lifespan relationship:

$$\lambda = c\sigma^q. \tag{17}$$

If q is <1, the increase in leaf lifespan slows down at high LMA; if q is >1, the increase in leaf lifespan accelerates at high LMA ($d\lambda/d\sigma = qc\sigma^{q-1}$). Based on this equation, we obtain a new equation for ESS LMA following the method used to derive Eqn (13) (ESS LMA):

$$\begin{aligned} N_{\mathrm{m}}^{\mathrm{ref}} &= \frac{N_{\mathrm{total}}}{(c\sigma_{\min}^{q-1}+s)\cdot\sigma_{\min}} \\ &= \frac{c+s\sigma^{*1-q}}{(c\sigma_{\min}^{q-1}+s)\cdot\sigma_{\min}}\cdot\frac{A+B\sigma^*}{kc} \\ &\quad\cdot\ln\left(\frac{Vc[qA\sigma^{*q-1}+(q-1)B\sigma^{*q}]}{(A+B\sigma^*)^2qrc\sigma^{*q-1}+GA}\right). \end{aligned} \tag{18}$$

This equation is the same as Eqn (13) when q is 1 (i.e., leaf lifespan changes with LMA isometrically). The patterns of ESS LMA are similar for different values of q (Fig. 4a). But, at a low reference N_{m} where ESS LMA exists, ESS LMA increases with q because the benefit gained from additional LMA increases as q increases.

Equation (3) implicitly assumes that the N which is proportional to LMA in Eqn (2) results in the same respiration rate as the N which is not. However, because leaf lifespan is proportional to LMA, whereas photosynthetic rate per unit leaf area is independent of LMA, a reasonable hypothesis is that some of the N which is proportional to LMA may not contribute to respiration because it is N in structural tissues like cell walls. We analyze the sensitivity of ESS LMA to alternative relationships between leaf respiration and leaf N by adding a parameter f to Eqn (3):

$$R = (A + fB\sigma)r, \tag{19}$$

where f ranges from 0 to 1. With Eqn (19), we obtain a new equation for ESS LMA:

$$\begin{aligned} N_{\mathrm{m}}^{\mathrm{ref}} &= \frac{N_{\mathrm{total}}}{(c+s)\sigma_{\min}} \\ &= \frac{(A+B\sigma_{\mathrm{ESS}})}{kc\sigma_{\min}}\cdot\ln\left(\frac{VAc}{cr(A^2+2fAB\sigma+fB^2\sigma^2)+AG}\right). \end{aligned} \tag{20}$$

This equation is the same as Eqn (13) if f is 1.0 (i.e., all leaf N has the same effect on respiration) (Fig. 4b). As f decreases, the ESS LMA increases at a given N availability because of decreases in maintenance cost. When f approaches zero (i.e., the N which is proportional to LMA does not contribute to respiration), ESS LMA goes to infinity (i.e., no ESS LMA) at the N availabilities lower than N_1 (Eqn 14) or goes to a bistable state (infinitely large or at minimum possible LMA) at the N availabilities higher than N_1.

Simulated forest succession patterns and final forest types by LM3-PPA

In the first set of simulation experiments, we assume a closed N cycle and vary total system nitrogen, holding all other parameters constant at the values of Harvard Forest (HFR). These simulation experiments simulate secondary succession at sites with different total nitrogen level. Using basal area of a PFT as the index of abundance, deciduous trees have a higher basal area than 'evergreen trees' at the beginning, but are soon exceeded by 'evergreen' trees at low ecosystem total N (170 gN m^{-2}) (Fig. 5a). At the medium total N (310 gN m^{-2}), 'evergreen' trees take more than 400 years to surpass deciduous trees' basal area (Fig. 5b). At high total N (710 gN m^{-2}), the basal area of deciduous trees is always higher than that of 'evergreen' trees (Fig. 5c).

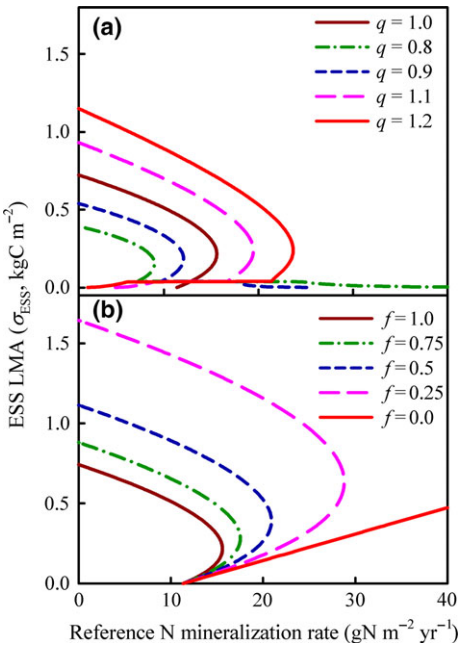

Fig. 4 Sensitivity of ESS LMA to physiological trade-offs between leaf lifespan and LMA (a) and between maintenance cost and leaf N in protective tissues (b). In panel (a), q is the exponent of LMA in the equation of leaf lifespan–LMA relationship ($\lambda = c\sigma^q$). In panel (b), f is the ratio of respiration induced by a unit of N which is proportional to LMA to that induced by a unit of N independent of LMA ($R = (A + fB\sigma)r$).

The N mineralization rate peaks in the early stage of ecosystem development, leading to higher LAI of deciduous than 'evergreen' canopy individuals initially (Fig. 5d–f). The very large spike in N mineralization in each run is the result of the initial condition that almost all ecosystem N is in undecomposed organic matter (Table S3 and Fig. S3). After the large initial spike in mineralized N, the N mineralization rate decreases as the stand develops, locking N in the fresh and high C : N ratio litter (Fig. S3). Eventually, in the low and medium N_{total} runs (170 and 310 gN m^{-2}, respectively), the LAI of deciduous trees becomes lower than that of 'evergreen' trees (Fig. 5d and e). At high total N (710 gN m^{-2}), the deciduous LAI is always higher than the 'evergreen' LAI because of the high N mineralization rate throughout the simulation (Fig. 5f).

In the second set of simulation experiments, we assume an open N cycle with a constant input rate and a temperature-dependent loss rate and vary site latitude, holding all other parameters constant (Fig. 6a–c). These simulation experiments simulate primary succession across a latitudinal gradient. The basal area of 'evergreen' trees is higher than that of deciduous trees in the early stages of forest succession at the three sites. The 'evergreen' trees are replaced by deciduous trees after a few decades of succession in the Oak Ridge simulations (OKR), the southern-most site (Fig. 6a). In the Harvard Forest simulations (HFR), deciduous trees take approximately 400 years to surpass the basal area of 'evergreen' trees (Fig. 6b). Finally, in the Northern Old Black Spruce site (NOBS) simulations, the northern-most site, the 'evergreen' trees dominate the site during the entire simulation and deciduous trees present at initialization are quickly driven extinct (Fig. 6c).

The dynamics of the N mineralization rate (Figs 5 and 6, blue lines in right panels) combined with our insights from the mathematical model provide the necessary insights to explain the patterns of 'evergreen' and deciduous abundance in the open N cycle simulations. The N mineralization rate at the end of a run is highest at OKR and lowest at NOBS (blue lines in Fig. 6d–f), consistent with the sites' differences in yearly mean temperatures. Individual LAIs of deciduous and 'evergreen' trees increase with time, consistent

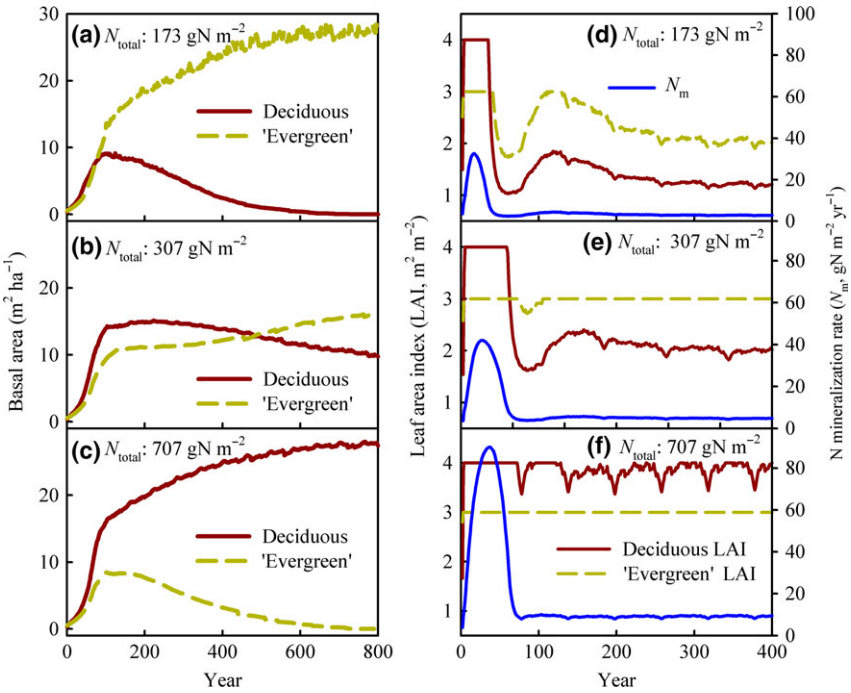

Fig. 5 Basal area, leaf area index (LAI), and N mineralization rate of canopy individuals from the simulation experiments with fixed ecosystem N at Harvard Forest. The panels of the left column (a, b, and c) show the simulated basal areas of 'evergreen' and deciduous PFTs at the total N of 170, 310, and 710 gN m^{-2}, respectively. The brown and green lines are the basal areas of deciduous and 'evergreen' trees, respectively. The panels of the right column (d, e, and f) show the annual N mineralization rate and LAIs of deciduous and 'evergreen' PFTs. The blue lines in the panels d, e, and f are the annual N mineralization rate (N_m). The brown and green lines are the LAIs of deciduous and 'evergreen' trees, respectively. The simulated N_m peaks in the early stages of ecosystem development, leading to greater LAI of deciduous trees than that of 'evergreen' trees. In later stages however, N_m decreases, making the LAI of deciduous trees lower than that of 'evergreen' trees in panels d and e. In panel f, where the N_{total} is the highest, the LAI of deciduous trees is always higher than that of 'evergreen' trees.

with the primary successional increase in the N mineralization rate at the three sites (blue lines Fig. 6d–f).

At OKR, the LAI of 'evergreen' trees is initially larger than that of deciduous trees because 'evergreen' trees require less N per leaf layer per year than deciduous trees (Fig. 6d). However, increasing N availability allows 'evergreens' to reach their light-limited maximum LAI within 100 years. The LAI of deciduous trees also starts low, but increases to its larger maximum value in about 300 years (Fig. 6d). The dynamics of N mineralization and LAI at HFR are qualitatively similar to OKR, but delayed in time due to the site's lower temperatures. At HFR, 'evergreen' trees require more than 100 years to reach maximum LAI and the deciduous nearly 600 (Fig. 6e). At NOBS, the coldest site, the N mineralization rate never reaches the level at which the deciduous is competitively dominant, and the 'evergreen' trees need about 200 years to reach to their maximum LAI (Fig. 6f).

It is important to understand that the fact that the 'evergreen' has a lower light-limited target LAI than the deciduous represents an *advantage* for the 'evergreen' not present in the mathematical model (where the forest is assumed to always be N-limited).

The diameter growth rates during the simulations reflect the changes in fitness through time as N availability changes (Fig. 7). Note, however, that the N mineralization rate above which deciduous trees grow faster than 'evergreens' differs among the simulations: roughly 4 gN m^{-2} yr^{-1} at OKR (Fig. 7a), 5 gN m^{-2} yr^{-1} at HFR (Fig. 7b), and 7–8 gN m^{-2} yr^{-1} at NOBS (Fig. 7c). This was not expected from the ESS analysis of the mathematical model and implies that the 'evergreen' PFT has additional relative advantages in cold sites, which are included in LM3-PPA, but not in the mathematical model. As described below, this is explained by the increased carbon-use efficiency (CUE) and early- and late-season photosynthesis of the 'evergreen' PFT, which has a relatively greater effect in the shorter growing season of colder climates.

We define CUE as the ratio of annual net primary production (NPP) to annual GPP in this study. Consistent with the theoretical predictions, the simulated CUE of deciduous trees is greater than that of 'evergreen'

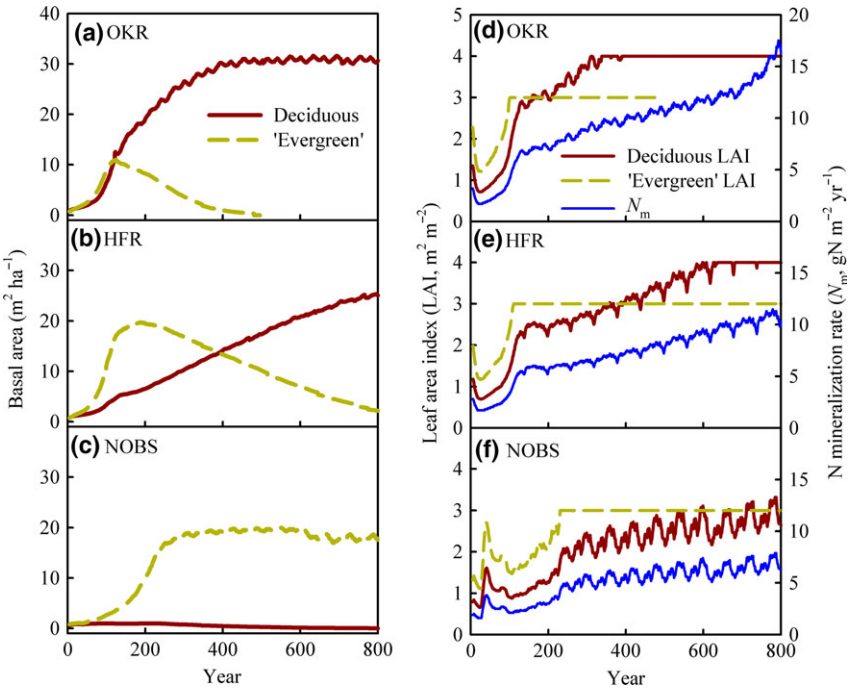

Fig. 6 Forest succession, N mineralization rate, and leaf area index (LAI) of the open N cycle simulation experiments. Panels a, b, and c are the simulated basal area of Oak Ridge (OKR) (a), Harvard Forest (HFR) (b), and the Northern Old Black Spruce site (NOBS) (c), respectively, representing the successional dynamics at the three sites ranging from most southerly (OKR) to most northerly (NOBS). The panels of the right column (d, e, and f) show the N mineralization rates and the LAIs of deciduous and 'evergreen' trees at the three sites. The solid blue lines represent N mineralization rates (N_m) at the three sites during the 800 simulation years. The solid brown and dashed light green lines are leaf area indexes of individual deciduous and 'evergreen' trees, respectively. The lines for LAI plateau with time as LAI reaches the light-limited LAI. The initial total N in these simulations is low (around 24 gN m^{-2}). The N input rate is 0.8 gN m^{-2} yr^{-1}, and N output depends on the temperature of the test sites. The yearly mean temperature decreases from OKR to NOBS (Table 3).

trees (Fig. 8a), and the simulated N-use efficiency (NUE, the ratio of annual NPP to annual N input to the canopy, i.e., the lifetime C return per unit N) of 'evergreen' trees is greater than that of deciduous trees (Fig. 8b) at all three sites. The higher LAI and eventual dominance by deciduous trees at OKR and HFR are due to the greater CUE of their low-LMA leaves. However, the difference in CUE between the two PFTs unexpectedly decreases with temperature from OKR to HFR to NOBS. This is evidence of an additional advantage of the 'evergreen' PFT in cold sites present in our new LM3-PPA that was not included in our mathematical model.

'Evergreen' trees have a longer growing season than the deciduous trees (Fig. 9a–c). This advantage is most significant in cold regions, where the growing season of deciduous trees is short and the added length of the 'evergreen' growing seasons creates the largest relative increase in carbon gain. This reduces the cost that species with high LMA pay for their added leaf respiration per unit leaf area and so decreases the leaf respiration advantage of low-LMA leaves (Fig. 9d–f). This explains why the difference between the CUEs of the 'evergreen' and deciduous PFTs decreases as mean temperature decreases from OKR to HFR to NOBS (Fig. 9d–f); it is because the CUE of the 'evergreen' increases faster than that of the deciduous PFT (Fig. 8a).

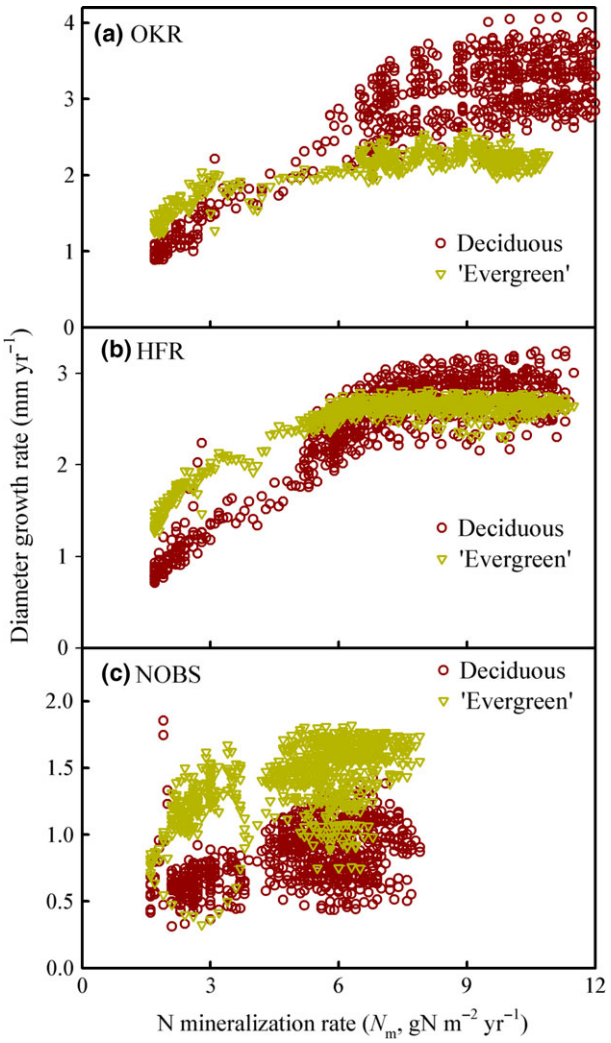

Fig. 7 Diameter growth rates from the open N cycle simulation experiments. Panels a, b, and c show the results of Oak Ridge (OKR), Harvard Forest (HFR), and the Northern Old Black Spruce (NOBS) sites, respectively. The diameter growth rate is the mean of the cohorts of a PFT (deciduous or 'evergreen') in the canopy layer. At a low N mineralization rate, the diameter growth rates of 'evergreen' trees are greater than those of deciduous trees at the three sites. At a high N mineralization rate however, the 'evergreen' trees grow more slowly than the deciduous trees at OKR and HFR.

Discussion

It has long been recognized that deciduous leaves tend to be more carbon efficient than evergreen leaves, whereas evergreen leaves tend to be more nutrient conservative, and that these differences work to determine the geographical distributions of the two types (Chabot & Hicks, 1982). Here, we show that empirical leaf trait relationships set up a trade-off between carbon- and nitrogen-use efficiency that can together explain the emergent property of observed distribution patterns of evergreen and deciduous trees in the temperate and boreal zones. Our simulation results imply that the primary and secondary succession on the relative dominance of evergreen and deciduous species may be caused by their adjustments to the NUE-CUE trade-off associated with LMA presented here.

Evolutionarily stable strategy analysis explains why short-lived leaves dominate when the rate of N mineralization is sufficiently high due to warm temperatures and/or N-rich soils, whereas long-lived leaves dominate where the rate of N mineralization is sufficiently low due to cold temperatures and/or N-poor soils. The simulation experiments show that an individual-based vegetation model with two PFTs differing only in leaf traits can generate realistic forest succession patterns in temperate and boreal regions, primarily because of the mechanisms identified in the mathematical model. These simulations suggest that the same mechanisms as revealed by the ESS analysis explain the dominance of deciduous trees early in secondary succession in the boreal zone when N availability is relatively high and the dominance of evergreens early in primary succession when N availability is low.

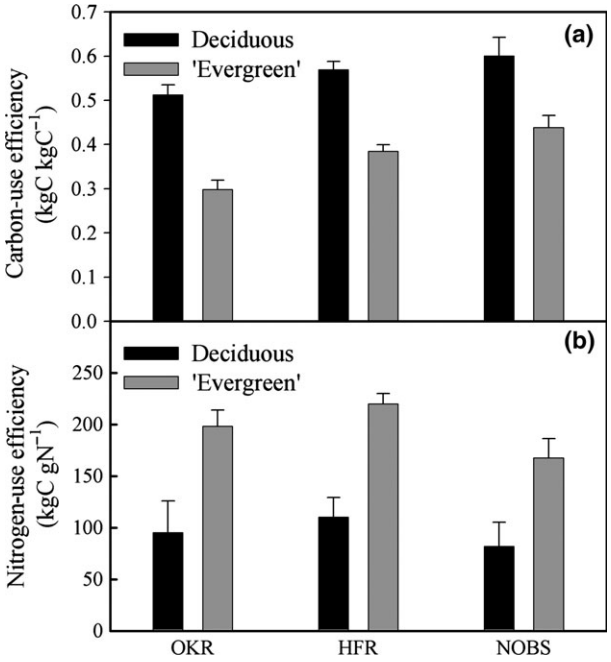

Fig. 8 Carbon- and N-use efficiencies from the open N cycle simulation experiments. Panel (a) shows the carbon-use efficiency (CUE), which is defined as the ratio of annual NPP to annual GPP, at Oak Ridge (OKR), Harvard Forest (HFR), and the Northern Old Black Spruce (NOBS) sites. Panel (b) shows the N-use efficiency (NUE), which is defined as the ratio of the NPP of a tree to the N allocated to new leaves from the N uptake by roots in a year at the three sites. The simulated CUE of deciduous trees is greater than that of 'evergreen' trees (a), whereas the simulated NUE of 'evergreen' trees is greater than that of deciduous trees (b) at all the three sites. The *difference* in CUE between these two PFTs decreases from OKR to HFR to NOBS.

Leaf traits, C- and N-use efficiency, and plant competition strategy

Both our mathematical model and simulation experiments are based on the same trade-offs of leaf traits (Eqns 1–3) discovered by analyses of global plant traits data (e.g., Wright *et al.*, 2004; Osnas *et al.*, 2013). Leaf photosynthesis capacity is almost entirely independent of LMA (Osnas *et al.*, 2013), making the dense conifer needles and thin broadleaf leaves approximately equivalent in photosynthetic capacity per unit leaf area (Reich *et al.*, 1995; Kattge *et al.*, 2009). However, the rate of net C gain per unit time of high-LMA leaves is lower than that of low-LMA leaves because of the high maintenance respiration of high-LMA leaves per unit area (Wright *et al.*, 2004; Osnas *et al.*, 2013). Although the carbon construction cost of a unit of leaf area is likely to be proportional to its LMA, the annualized construction cost is likely to be independent of LMA because leaf lifespan is proportional to LMA (LMA/Leaf life span = $1/c$) (Wright *et al.*, 2004). Together, these relationships imply that the rate of carbon return on a carbon investment in leaves (i.e., CUE) decreases as LMA increases. Contrary to CUE, the NUE increases as LMA increases. The annualized N cost of a unit of leaf area decreases as LMA increases (Leaf N/Leaf life span = $A/c\sigma + B/c$). Thus, the longevity of evergreen leaves allows evergreen trees to maintain higher LAI than deciduous trees in N-limited ecosystems (Gower *et al.*, 1993) and higher lifetime return in carbon (Falster *et al.*, 2012). Overall, high-LMA leaves have high NUE because of their long lifespan but low CUE because of their high maintenance cost.

The differences in CUE and NUE explain why deciduous trees win in N-rich soils, whereas evergreen trees win in N-poor soils. At low N availability, high-LMA trees have higher net C gain than low-LMA trees because their N retention allows them to maintain more leaf layers (i.e., higher LAI). High N availability eliminates or reverses the LAI advantage of high-LMA species and favors the CUE advantage of low-LMA species. Thus, the leaf trait relationships in our mathematical model and simulation experiments cause a trade-off between the productivity of each leaf layer and the number of leaf layers that a tree can produce when N is limiting.

Model structural sensitivity and uncertainty

Variations in the relationships between LMA and leaf lifespan and between leaf respiration and leaf N do not change the qualitative results about the ESS of LMA (Fig. 4), but they do change the relative costs and benefits of leaves with different LMAs and thus the quantitative patterns. For example, if the marginal leaf lifespan increases as LMA increases (e.g., $q > 1$), ESS LMA tends to be high. Similarly, if the marginal respiratory cost of LMA is low (e.g., $f < 1$), the ESS LMA will also be high. An ESS LMA does not exist only when the protective tissues have no maintenance cost (i.e., $f = 0$). However, variation in LMA involves changes in mesophyll cells (Poorter *et al.*, 2009; Villar *et al.*, 2013), suggesting that the N which is proportional to LMA must come at a respiration cost, although its contribution to the total respiration rate may be lower than that of N (which is independent of LMA). These sensitivity analyses indicate that the model only requires monotonically increasing relationships between LMA and leaf lifespan and between leaf respiration and leaf N to create a trade-off between CUE and NUE. The ESS represented in Eqn (13) is the simplest case that assumes leaf lifespan is proportional to LMA and the structural N has the same respiration coefficient with functional N (Eqns 1 and 3).

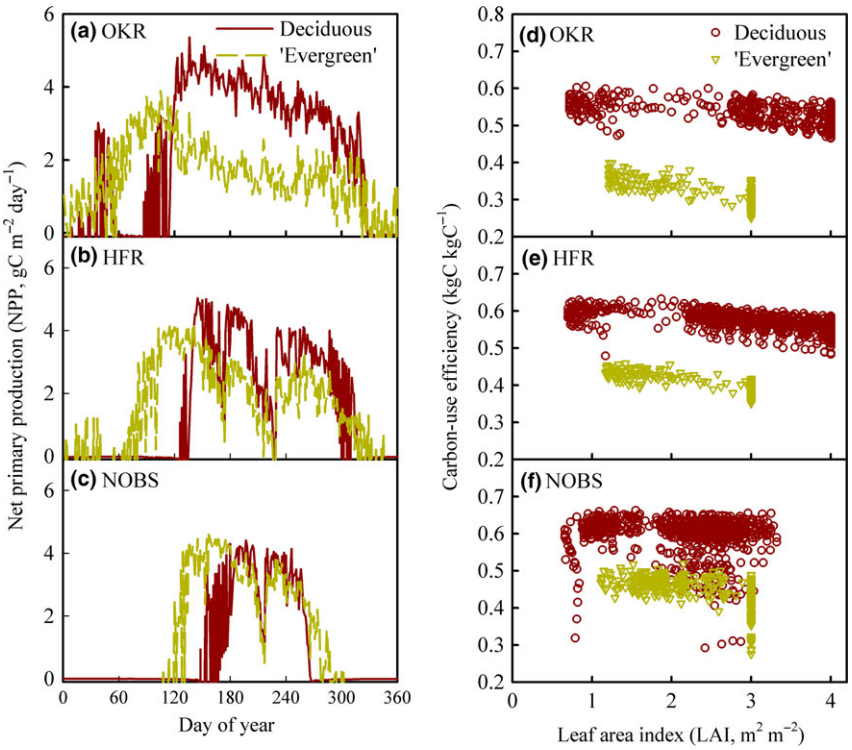

Fig. 9 Simulated net primary production (NPP) and carbon-use efficiency (CUE) from the open N cycle simulation experiments. Panels a, b, and c show the daily NPP of deciduous and 'evergreen' trees at Oak Ridge (OKR), Harvard Forest (HFR), and the Northern Old Black Spruce (NOBS) sites, respectively, illustrating that 'evergreen' trees have a longer growing season than the deciduous trees. Panels d, e, and f show the differences between the CUEs of deciduous and 'evergreen' trees as LAI increases at the three sites, respectively. The *difference* between the CUEs of the 'evergreen' and deciduous PFTs decreases as mean temperature decreases from OKR to HFR to NOBS because the CUE of the 'evergreen' increases faster than that of the deciduous PFT.

An additional factor included in the simulation experiments, but not in the mathematical model, is that the low respiration rate of low-LMA leaves means that low-LMA trees can maintain more leaf layers with positive carbon balance than high-LMA trees when the N supply is sufficient to produce the extra layers (i.e., the high LAI of deciduous trees at high N availability as shown in Fig. 6d–f). This reinforces the inverse relationship between CUE and LMA. A factor not included in either the mathematical model or simulation experiments is the decline of the gross and net photosynthetic rates as a leaf ages (Wilson *et al.*, 2000; Kitajima *et al.*, 2002; Warren, 2006), which would also strengthen the inverse relationship between CUE and LMA.

Bistable state

The positive feedback between LMA and the rate of decomposition of SOM (Cornwell *et al.*, 2008; Zhang *et al.*, 2008) leads to the prediction of founder control by the mathematical model at intermediate N availability (intermediate values of N_m^{ref}). High-N litter produced by a low-LMA species accelerates decomposition and thus increases N mineralization rate, which competitively favors a species with an even lower LMA. Similarly, low-N litter produced by high-LMA species reduces N mineralization rate, which competitively favors an even higher LMA. With founder control, one expects a patchy mosaic of a high-LMA PFT with long-lived leaves and a low-LMA PFT with short-lived leaves that reflects patchy initial conditions. A very similar explanation was proposed by Pastor & Post (1986) for the patchy mix of evergreen confers and broadleaf species on Black Hawk Island (Pastor *et al.*, 1982) and by Gower & Richards (1990) for the patchy coexistence of deciduous larches and birches with evergreen conifers throughout the boreal zone. Although we observed no evidence of founder control in the simulation model, we did not systematically search for it.

Simulated forest succession, C- and N-use strategy, and temperature effects

The simulated secondary (closed N cycle runs) succession (Fig. 5a–c) and primary (open N cycle runs) succession (Fig. 6a–c) by the LM3-PPA are consistent with

those reported in the literature (Gower & Richards, 1990; Givnish, 2002). In particular, secondary succession from deciduous to evergreen dominance is consistent with field observations in regions where confers are the late-successional dominants. In boreal forests, recovery after a large disturbance event (e.g., fire) is usually pioneered by deciduous trees (e.g., *Betula* spp. and *Larix* spp.), which are subsequently replaced by evergreen conifer trees (*Pinus*, *Abies*, and *Picea*) (Chapin *et al*., 1994; Lichter, 1998; Schulze *et al*., 2005). The simulated pattern of N mineralization during secondary succession (Fig. 5d–f), which causes the progression from deciduous to evergreen dominance, is also consistent with field measurements. The N mineralization rate is usually high after a stand-replacing disturbance event (Deng *et al*., 2014) and then gradually decreases with the replacement of early species by late species (Vitousek *et al*., 1989; Vancleve *et al*., 1993). The simulation experiments predict dominance by evergreens late in secondary succession wherever the N mineralization rate falls beneath the threshold below which evergreens become competitively dominant (Fig. 5d and e) and dominance by deciduous trees if the N mineralization rate stays above this threshold (Fig. 5f).

During primary succession, the simulation experiments predict evergreen trees early in succession and a shift to deciduous dominance in the temperate zone because the buildup of total ecosystem N eventually drives the N mineralization rate above the threshold for deciduous dominance (Fig. 6). Elsewhere, the N mineralization rate stays low enough throughout primary succession so that evergreens remain dominant. These patterns are consistent with observations. For example, primary succession in the Southern Lake Michigan sand dunes is from evergreen conifers, for example, jack or white pine (*Pinus banksiana*, *P. strobus*), to broadleaf deciduous, for example, black oak (*Quercus velutina*) (Olson, 1958).

Temperature drives the distribution of deciduous and evergreen forests in both the mathematical model and the simulation experiments because the N mineralization rates that define the distributions of evergreen and deciduous forests are strongly dependent on temperature. Similarly, in traditional DGVMs, temperature is directly used to select leaf traits, limiting the distributions of deciduous and evergreen tree PFTs. However, in our model, temperature affects the outcome of competition primarily because it changes the N mineralization rate. In the simulation experiments with an open N cycle, temperature also affects how much N builds up in an ecosystem because it affects leaching and dissolved organic nitrogen losses by affecting evapotranspiration and thus runoff and by directly affecting the rate of denitrification (see Appendix S1).

Evolutionarily stable strategy and site productivity

Usually, the models that predict optimal trait combinations in different environments assume the strategies (i.e., combinations of plant traits) that lead to high productivity will be dominant (e.g., Haxeltine & Prentice, 1996; Kleidon & Mooney, 2000; Pavlick *et al*., 2013; van Bodegom *et al*., 2014). However, as shown in this study, the more ecologically relevant ESS of LMA does not always maximize the stand's net C gain because ESS excludes the trait combinations that are ineffective competitively. For example, at a low N_m^{ref} (i.e., the total N of 100 gN m^{-2}, Fig. S4a), any resident LMA below the ESS can always be invaded by a slightly higher LMA, which is closer to the ESS value (Fig. S4a). In this case, the net C gain of the resident decreases as its LMA increases (Fig. S4b) and so the succession of residents on the approach to the ESS is associated with a monotonic decrease in canopy net carbon gain (Fig. S4b). Invasion succeeds despite this decrease because invaders with LMAs closer to the ESS value have higher C gain than the resident at the N mineralization rate created by the resident's leaf litter (Fig. S4b). But once the old resident is replaced by the invader and the N mineralization rate has equilibrated to its new lower value (because of the higher C : N ratio of the higher LMA litter), the net C gain of the forest under the new resident is less than it was under the old resident. This is a partial tragedy of the commons driven by shared access to resources (Hardin, 1968; Gersani *et al*., 2001; Rankin *et al*., 2007; McNickle & Dybzinski, 2013; Farrior, 2014).

Acknowledgements

Funding was provided by USDA Forest Service Northern Research Station (Agreement 13-JV-11242315-066) and Princeton Environment Institute. We thank Dr. Sergey Malyshev for his help in preparing forcing data and Dr. Cleo Chou for her helpful comments on an earlier version of this manuscript. We thank Prof. I. Colin Prentice and other three reviewers for their insightful comments and suggestions, which greatly improved this manuscript. This work was conducted while CEF was a postdoctoral fellow at the National Institute for Mathematical and Biological Synthesis, sponsored by the National Science Foundation through NSF Award #DBI-1300426, with additional support from The University of Tennessee, Knoxville.

References

Abrams MD (1998) The red maple paradox. *BioScience*, **48**, 355–364.

Ackerly DD (2003) Community assembly, niche conservatism, and adaptive evolution in changing environments. *International Journal of Plant Sciences*, **164**, S165–S184.

Anten NPR (2002) Evolutionarily stable leaf area production in plant populations. *Journal of Theoretical Biology*, **217**, 15–32.

Bergeron O, Margolis HA, Black TA, Coursolle C, Dunn AL, Barr AG, Wofsy SC (2007) Comparison of carbon dioxide fluxes over three boreal black spruce forests in Canada. *Global Change Biology*, **13**, 89–107.

van Bodegom PM, Douma JC, Verheijen LM (2014) A fully traits-based approach to modeling global vegetation distribution. *Proceedings of the National Academy of Sciences of the United States of America*, **111**, 13733–13738.

Chabot BF, Hicks DJ (1982) The ecology of leaf life spans. *Annual Review of Ecology and Systematics*, **13**, 229–259.

Chapin FS, Walker LR, Fastie CL, Sharman LC (1994) Mechanisms of primary succession following deglaciation at Glacier Bay, Alaska. *Ecological Monographs*, **64**, 149–175.

Cornwell WK, Cornelissen JHC, Amatangelo K *et al*. (2008) Plant species traits are the predominant control on litter decomposition rates within biomes worldwide. *Ecology Letters*, **11**, 1065–1071.

Curtis PS, Hanson PJ, Bolstad P, Barford C, Randolph JC, Schmid HP, Wilson KB (2002) Biometric and eddy-covariance based estimates of annual carbon storage in five eastern North American deciduous forests. *Agricultural and Forest Meteorology*, **113**, 3–19.

Davis MB (1986) Climatic instability, time lags and community disequilibrium. In: *Community Ecology* (eds Diamond J, Case TJ), pp. 269–284. Harper and Row, New York.

Deng Q, Cheng XL, Yang YH, Zhang QF, Luo YQ (2014) Carbon-nitrogen interactions during afforestation in central China. *Soil Biology & Biochemistry*, **69**, 119–122.

Dunn AL, Barford CC, Wofsy SC, Goulden ML, Daube BC (2007) A long-term record of carbon exchange in a boreal black spruce forest: means, responses to interannual variability, and decadal trends. *Global Change Biology*, **13**, 577–590.

Duursma RA, Makela A (2007) Summary models for light interception and light-use efficiency of non-homogeneous canopies. *Tree Physiology*, **27**, 859–870.

Dybzinski R, Farrior C, Wolf A, Reich PB, Pacala SW (2011) Evolutionarily stable strategy carbon allocation to foliage, wood, and fine roots in trees competing for light and nitrogen: an analytically tractable, individual-based model and quantitative comparisons to data. *The American Naturalist*, **177**, 153–166.

Dybzinski R, Farrior CE, Ollinger S, Pacala SW (2013) Interspecific vs intraspecific patterns in leaf nitrogen of forest trees across nitrogen availability gradients. *New Phytologist*, **200**, 112–121.

Dybzinski R, Farrior CE, Pacala SW (2015) Increased forest carbon storage with increased atmospheric CO_2 despite nitrogen limitation: a game-theoretic allocation model for trees in competition for nitrogen and light. *Global Change Biology*, **21**, 1182–1196.

Evans JR, Poorter H (2001) Photosynthetic acclimation of plants to growth irradiance: the relative importance of specific leaf area and nitrogen partitioning in maximizing carbon gain. *Plant, Cell and Environment*, **24**, 755–767.

Falster DS, Westoby M (2003) Plant height and evolutionary games. *Trends in Ecology & Evolution*, **18**, 337–343.

Falster DS, Reich PB, Ellsworth DS, Wright IJ, Westoby M, Oleksyn J, Lee TD (2012) Lifetime return on investment increases with leaf lifespan among 10 Australian woodland species. *New Phytologist*, **193**, 409–419.

Farrior CE (2014) Competitive optimization models, attempting to understand the diversity of life. *New Phytologist*, **203**, 1025–1027.

Farrior CE, Dybzinski R, Levin SA, Pacala SW (2013a) Competition for water and light in closed-canopy forests: a tractable model of carbon allocation with implications for carbon sinks. *The American Naturalist*, **181**, 314–330.

Farrior CE, Tilman D, Dybzinski R, Reich PB, Levin SA, Pacala SW (2013b) Resource limitation in a competitive context determines complex plant responses to experimental resource additions. *Ecology*, **94**, 2505–2517.

Field C (1983) Allocating leaf nitrogen for the maximization of carbon gain – leaf age as a control on the allocation program. *Oecologia*, **56**, 341–347.

Foley JA, Levis S, Prentice IC, Pollard D, Thompson SL (1998) Coupling dynamic models of climate and vegetation. *Global Change Biology*, **4**, 561–579.

Foley JA, Levis S, Costa MH, Cramer W, Pollard D (2000) Incorporating dynamic vegetation cover within global climate models. *Ecological Applications*, **10**, 1620–1632.

Garnier E, Cortez J, Billes G *et al*. (2004) Plant functional markers capture ecosystem properties during secondary succession. *Ecology*, **85**, 2630–2637.

Gerber S, Hedin LO, Oppenheimer M, Pacala SW, Shevliakova E (2010) Nitrogen cycling and feedbacks in a global dynamic land model. *Global Biogeochemical Cycles*, **24**, GB1001.

Geritz SAH, Kisdi E, Meszena G, Metz JAJ (1998) Evolutionarily singular strategies and the adaptive growth and branching of the evolutionary tree. *Evolutionary Ecology*, **12**, 35–57.

Gersani M, Brown JS, O'Brien EE, Maina GM, Abramsky Z (2001) Tragedy of the commons as a result of root competition. *Journal of Ecology*, **89**, 660–669.

Givnish TJ (2002) Adaptive significance of evergreen vs. deciduous leaves: solving the triple paradox. *Silva Fennica*, **36**, 703–743.

Goetz SJ, Prince SD (1999) Modelling terrestrial carbon exchange and storage: evidence and implications of functional convergence in light-use efficiency. *Advances in Ecological Research*, **28**, 57–92.

Gower ST, Richards JH (1990) Larches – deciduous conifers in an evergreen world. *BioScience*, **40**, 818–826.

Gower ST, Reich PB, Son Y (1993) Canopy dynamics and aboveground production of 5 tree species with different leaf longevities. *Tree Physiology*, **12**, 327–345.

Hardin G (1968) The tragedy of the commons. *Science*, **162**, 1243–1248.

Haxeltine A, Prentice IC (1996) BIOME3: an equilibrium terrestrial biosphere model based on ecophysiological constraints, resource availability, and competition among plant functional types. *Global Biogeochemical Cycles*, **10**, 693–709.

Hikosaka K, Hirose T (1997) Leaf angle as a strategy for light competition: optimal and evolutionarily stable light-extinction coefficient within a leaf canopy. *Ecoscience*, **4**, 501–507.

Kattge J, Knorr W, Raddatz T, Wirth C (2009) Quantifying photosynthetic capacity and its relationship to leaf nitrogen content for global-scale terrestrial biosphere models. *Global Change Biology*, **15**, 976–991.

King DA (1990) The adaptive significance of tree height. *The American Naturalist*, **135**, 809–828.

Kitajima K, Mulkey SS, Samaniego M, Wright SJ (2002) Decline of photosynthetic capacity with leaf age and position in two tropical pioneer tree species. *American Journal of Botany*, **89**, 1925–1932.

Kleidon A, Mooney HA (2000) A global distribution of biodiversity inferred from climatic constraints: results from a process-based modelling study. *Global Change Biology*, **6**, 507–523.

Landsberg JJ, Waring RH (1997) A generalised model of forest productivity using simplified concepts of radiation-use efficiency, carbon balance and partitioning. *Forest Ecology and Management*, **95**, 209–228.

Laughlin DC, Laughlin DE (2013) Advances in modeling trait-based plant community assembly. *Trends in Plant Science*, **18**, 584–593.

Lichter J (1998) Primary succession and forest development on coastal Lake Michigan sand dunes. *Ecological Monographs*, **68**, 487–510.

Lichter J, Billings SA, Ziegler SE *et al*. (2008) Soil carbon sequestration in a pine forest after 9 years of atmospheric CO(2) enrichment. *Global Change Biology*, **14**, 2910–2922.

Lloyd J, Bloomfield K, Domingues TF, Farquhar GD (2013) Photosynthetically relevant foliar traits correlating better on a mass vs an area basis: of ecophysiological relevance or just a case of mathematical imperatives and statistical quicksand? *New Phytologist*, **199**, 311–321.

Manzoni S, Trofymow JA, Jackson RB, Porporato A (2010) Stoichiometric controls on carbon, nitrogen, and phosphorus dynamics in decomposing litter. *Ecological Monographs*, **80**, 89–106.

Maynard Smith J (1974) Theory of games and evolution of animal conflicts. *Journal of Theoretical Biology*, **47**, 209–221.

Mcclaugherty CA, Pastor J, Aber JD, Melillo JM (1985) Forest litter decomposition in relation to soil-nitrogen dynamics and litter quality. *Ecology*, **66**, 266–275.

McNickle GG, Dybzinski R (2013) Game theory and plant ecology. *Ecology Letters*, **16**, 545–555.

Medlyn BE, Badeck FW, De Pury DGG *et al*. (1999) Effects of elevated [CO2] on photosynthesis in European forest species: a meta-analysis of model parameters. *Plant, Cell and Environment*, **22**, 1475–1495.

Medvigy D, Wofsy SC, Munger JW, Hollinger DY, Moorcroft PR (2009) Mechanistic scaling of ecosystem function and dynamics in space and time: Ecosystem Demography model version 2. *Journal of Geophysical Research-Biogeosciences*, **114**, G01002.

Monteith JL (1977) Climate and efficiency of crop production in Britain. *Philosophical Transactions of the Royal Society of London Series B: Biological Sciences*, **281**, 277–294.

Moorcroft PR, Hurtt GC, Pacala SW (2001) A method for scaling vegetation dynamics: the ecosystem demography model (ED). *Ecological Monographs*, **71**, 557–585.

Nagel JM, Griffin KL, Schuster WSF, Tissue DT, Turnbull MH, Brown KJ, Whitehead D (2002) Energy investment in leaves of red maple and co-occurring oaks within a forested watershed. *Tree Physiology*, **22**, 859–867.

Norby RJ, Todd DE, Fults J, Johnson DW (2001) Allometric determination of tree growth in a CO_2-enriched sweetgum stand. *New Phytologist*, **150**, 477–487.

Olson JS (1958) Rates of succession and soil changes on Southern Lake Michigan sand dunes. *Botanical Gazette*, **119**, 125–170.

Osnas JLD, Lichstein JW, Reich PB, Pacala SW (2013) Global leaf trait relationships: mass, area, and the leaf economics spectrum. *Science*, **340**, 741–744.

Pappas C, Fatichi S, Burlando P (2016) Modeling terrestrial carbon and water dynamics across climatic gradients: does plant trait diversity matter? *New Phytologist*, **209**, 137–151.

Pastor J, Post WM (1986) Influence of climate, soil-moisture, and succession on forest carbon and nitrogen cycles. *Biogeochemistry*, **2**, 3–27.

Pastor J, Aber JD, Mcclaugherty CA, Melillo JM (1982) Geology, soils and vegetation of Blackhawk Island, Wisconsin. *American Midland Naturalist*, **108**, 266–277.

Pavlick R, Drewry DT, Bohn K, Reu B, Kleidon A (2013) The Jena Diversity-Dynamic Global Vegetation Model (JeDi-DGVM): a diverse approach to representing terrestrial biogeography and biogeochemistry based on plant functional trade-offs. *Biogeosciences*, **10**, 4137–4177.

Pearcy RW, Bjorkman O, Caldwell MM, Keeley JE, Monson RK, Strain BR (1987) Carbon gain by plants in natural environments. *BioScience*, **37**, 21–29.

Poorter H, Niinemets U, Poorter L, Wright IJ, Villar R (2009) Causes and consequences of variation in leaf mass per area (LMA): a meta-analysis. *New Phytologist*, **182**, 565–588.

Prentice IC, Cramer W, Harrison SP, Leemans R, Monserud RA, Solomon AM (1992) A global biome model based on plant physiology and dominance, soil properties and climate. *Journal of Biogeography*, **19**, 117–134.

Rankin DJ, Bargum K, Kokko H (2007) The tragedy of the commons in evolutionary biology. *Trends in Ecology & Evolution*, **22**, 643–651.

Reich PB, Kloeppel BD, Ellsworth DS, Walters MB (1995) Different photosynthesis-nitrogen relations in deciduous hardwood and evergreen coniferous tree species. *Oecologia*, **104**, 24–30.

Reich PB, Ellsworth DS, Walters MB (1998a) Leaf structure (specific leaf area) modulates photosynthesis-nitrogen relations: evidence from within and across species and functional groups. *Functional Ecology*, **12**, 948–958.

Reich PB, Walters MB, Ellsworth DS, Vose JM, Volin JC, Gresham C, Bowman WD (1998b) Relationships of leaf dark respiration to leaf nitrogen, specific leaf area and leaf life-span: a test across biomes and functional groups. *Oecologia*, **114**, 471–482.

Reich PB, Ellsworth DS, Walters MB, Vose JM, Gresham C, Volin JC, Bowman WD (1999) Generality of leaf trait relationships: a test across six biomes. *Ecology*, **80**, 1955–1969.

Reich PB, Rich RL, Lu XJ, Wang YP, Oleksyn J (2014) Biogeographic variation in evergreen conifer needle longevity and impacts on boreal forest carbon cycle projections. *Proceedings of the National Academy of Sciences of the United States of America*, **111**, 13703–13708.

Reu B, Proulx R, Bohn K, Dyke JG, Kleidon A, Pavlick R, Schmidtlein S (2011) The role of climate and plant functional trade-offs in shaping global biome and biodiversity patterns. *Global Ecology and Biogeography*, **20**, 570–581.

Sakschewski B, von Bloh W, Boit A *et al.* (2015) Leaf and stem economics spectra drive diversity of functional plant traits in a dynamic global vegetation model. *Global Change Biology*, **21**, 2711–2725.

Savage KE, Davidson EA (2001) Interannual variation of soil respiration in two New England forests. *Global Biogeochemical Cycles*, **15**, 337–350.

Scheiter S, Langan L, Higgins SI (2013) Next-generation dynamic global vegetation models: learning from community ecology. *New Phytologist*, **198**, 957–969.

Schulze ED, Wirth C, Mollicone D, Ziegler W (2005) Succession after stand replacing disturbances by fire, wind throw, and insects in the dark Taiga of Central Siberia. *Oecologia*, **146**, 77–88.

Sheffield J, Goteti G, Wood EF (2006) Development of a 50-year high-resolution global dataset of meteorological forcings for land surface modeling. *Journal of Climate*, **19**, 3088–3111.

Shipley B, Vile D, Garnier E (2006) From plant traits to plant communities: a statistical mechanistic approach to biodiversity. *Science*, **314**, 812–814.

Sitch S, Smith B, Prentice IC *et al.* (2003) Evaluation of ecosystem dynamics, plant geography and terrestrial carbon cycling in the LPJ dynamic global vegetation model. *Global Change Biology*, **9**, 161–185.

Vancleve K, Yarie J, Erickson R, Dyrness CT (1993) Nitrogen mineralization and nitrification in successional ecosystems on the Tanana River floodplain, interior Alaska. *Canadian Journal of Forest Research - Revue Canadienne De Recherche Forestiere*, **23**, 970–978.

Verheijen LM, Brovkin V, Aerts R *et al.* (2013) Impacts of trait variation through observed trait-climate relationships on performance of an Earth system model: a conceptual analysis. *Biogeosciences*, **10**, 5497–5515.

Verheijen LM, Aerts R, Brovkin V, Cavender-Bares J, Cornelissen JHC, Kattge J, Van Bodegom PM (2015) Inclusion of ecologically based trait variation in plant functional types reduces the projected land carbon sink in an earth system model. *Global Change Biology*, **21**, 3074–3086.

Vermeulen PJ (2014) Crown depth as a result of evolutionary games: decreasing solar angle should lead to shallower, not deeper crowns. *New Phytologist*, **202**, 1249–1256.

Villar R, Ruiz-Robleto J, Ubera JL, Poorter H (2013) Exploring variation in leaf mass per area (LMA) from leaf to cell: an anatomical analysis of 26 woody species. *American Journal of Botany*, **100**, 1969–1980.

Violle C, Reich PB, Pacala SW, Enquist BJ, Kattge J (2014) The emergence and promise of functional biogeography. *Proceedings of the National Academy of Sciences of the United States of America*, **111**, 13690–13696.

Vitousek PM, Matson PA, van Cleve K (1989) Nitrogen availability and nitrification during succession: primary, secondary, and old-field seres. *Plant and Soil*, **115**, 229–239.

Wang YP, Lu XJ, Wright IJ, Dai YJ, Rayner PJ, Reich PB (2012) Correlations among leaf traits provide a significant constraint on the estimate of global gross primary production. *Geophysical Research Letters*, **39**, L19405. doi:10.1029/2012gl053461.

Warren CR (2006) Why does photosynthesis decrease with needle age in *Pinus pinaster*? *Trees-Structure and Function*, **20**, 157–164.

Weiher E, Freund D, Bunton T, Stefanski A, Lee T, Bentivenga S (2011) Advances, challenges and a developing synthesis of ecological community assembly theory. *Philosophical Transactions of the Royal Society of London Series B: Biological Sciences*, **366**, 2403–2413.

Weng ES, Malyshev S, Lichstein JW *et al.* (2015) Scaling from individual trees to forests in an Earth system modeling framework using a mathematically tractable model of height-structured competition. *Biogeosciences*, **12**, 2655–2694.

Wilson KB, Baldocchi DD, Hanson PJ (2000) Spatial and seasonal variability of photosynthetic parameters and their relationship to leaf nitrogen in a deciduous forest. *Tree Physiology*, **20**, 565–578.

Wright IJ, Reich PB, Westoby M *et al.* (2004) The worldwide leaf economics spectrum. *Nature*, **428**, 821–827.

Wright IJ, Reich PB, Cornelissen JHC *et al.* (2005) Assessing the generality of global leaf trait relationships. *New Phytologist*, **166**, 485–496.

Wullschleger SD, Epstein HE, Box EO *et al.* (2014) Plant functional types in Earth system models: past experiences and future directions for application of dynamic vegetation models in high-latitude ecosystems. *Annals of Botany*, **114**, 1–16.

Zhang D, Hui DF, Luo YQ, Zhou GY (2008) Rates of litter decomposition in terrestrial ecosystems: global patterns and controlling factors. *Journal of Plant Ecology*, **1**, 85–93.

Supporting Information

Additional Supporting Information may be found in the online version of this article:

Appendix S1. Nitrogen cycle and allocation scheme in the LM3-PPA model.
Appendix S2. Mathematical derivations of Evolutionarily Stable Strategy of LMA.
Table S1. Parameters of the N model in LM3-PPA.
Table S2. Initial conditions for the N-open runs at the three forest sites, Oak Ridge (OKR), Harvard Forest (HFR), Northern Old Black Spruce Site (NOBS).
Table S3. Initial carbon and nitrogen pools for the N-closed runs at Harvard Forest (HFR).
Figure S1. Pairwise invasion plots of LMA strategies across a gradient in total N.
Figure S2. Schematic diagram of predicted deciduous and evergreen forest distribution along the axes of temperature and soil nitrogen content.
Figure S3. Redistribution of nitrogen stocks and N mineralization rate during the process of secondary succession in N-closed runs.
Figure S4. Net carbon gain at optimal and ESS LMA.